A Fast Mollified Impulse Method for Biomolecular Atomistic Simulations

L. Fath[a,*], M. Hochbruck[a], C.V. Singh[b]

[a] *Institute for App. and Num. Mathematics, Karlsruhe Institute of Technology, Germany*
[b] *Department of Materials Science & Engineering, University of Toronto, Canada*

Abstract

Classical integration methods for molecular dynamics are inherently limited due to resonance phenomena occurring at certain time-step sizes. The mollified impulse method can partially avoid this problem by using appropriate filters based on averaging or projection techniques. However, existing filters are computationally expensive and tedious in implementation since they require either analytical Hessians or they need to solve nonlinear systems from constraints. In this work we follow a different approach based on corotation for the construction of a new filter for (flexible) biomolecular simulations. The main advantages of the proposed filter are its excellent stability properties and ease of implementation in standard softwares without Hessians or solving constraint systems. By simulating multiple realistic examples such as peptide, protein, ice equilibrium and ice-ice friction, the new filter is shown to speed up the computations of long-range interactions by approximately 20%. The proposed filtered integrators allow step sizes as large as 10 fs while keeping the energy drift less than 1% on a 50 ps simulation.

Keywords: mollified impulse method, highly oscillatory, resonances, corotation, molecular dynamics

1. Introduction

The tremendous rise of available computing power has made simulations based on classical molecular dynamics (MD) a powerful tool for many investigations such as predicting material properties. Those simulations are fruitful in research of mechanisms on a nanoscale and allow for deeper insight on how exactly many phenomena occur. However, the simulations itself are computationally challenging; both time scale and physical scale are so small that investigations usually have to be restricted to very small domains and very short time frames [1–3].

*Corresponding author
Email addresses: lukas.fath@kit.edu (L. Fath), marlis.hochbruck@kit.edu (M. Hochbruck), chandraveer.singh@utoronto.ca (C.V. Singh)

Multiple time-step (MTS) approaches [4–8] can significantly increase the accessible time scale by taking advantage of the specific structure of the underlying problem. Standard MTS methods, such as the impulse method [9, 10], increase computational efficiency by evaluating force fields only at their corresponding time scale. Unfortunately, highly oscillatory motions lead to severe resonance instabilities in standard integrators which restrict their step sizes [11–16] to below 5fs for most problems. Especially the expensive computation of slow, but long-range electrostatic contributions still poses a major bottleneck in many simulations. Therefore, achieving a larger outer time-step in MTS integrators is a pressing objective of research.

For equilibrium simulations, such as sampling conformational equilibria, multiple and very successful attempts to tackle the time scale problem have been proposed; a clever restriction of certain parameters with thermostats, averaging techniques, and adding stochastic forces make it possible to avoid resonance problems [17–19], and step sizes of 100fs and larger have been reported. However, these methods do not preserve the dynamics, since a large number of constraints is used to impede energy build-ups in single modes.

Hence, for non-equilibrium simulations, such as dynamic processes like friction, phase transformations, or grain boundaries, the dynamics itself make it questionable to use such methods [20, 21]. One possibility here is to freeze the fastest degrees of freedom with algorithms such as SHAKE [22, 23]. However, this rather drastic step removes all contributions which are attributed to the fastest modes. Instead, mild stochastic forces can be used [24–26], but care has to be taken to choose a weak coupling to not destroy the dynamics. The mollified impulse method [27] uses a totally different idea. Resonances are avoided using averaged positions for the evaluation of the slowest potential. In contrast to SHAKE, this method retains its ability to resolve the fastest frequencies. Furthermore, this approach can be carefully combined with methods using mild stochastic forces [28, 29] reaching even longer time-steps.

A crucial ingredient of the mollified impulse method is its filter. Current filters are either based on averaging [15] or projection [30, 31] techniques. Averaging techniques have been analyzed [32] and tested on small systems [33]. Their major drawback is expensive forward and backward integration with analytical Hessians of the oscillatory part of the potential. Furthermore, numerical experiments [30, 34] suggest that these methods are less stable than projection methods where molecules are projected back to their rest positions. However, this requires solving a nonlinear constraint system with SHAKE-like Newton iterations in each time-step.

In this paper we present a new filter technique based on corotation. It is designed for biomolecular simulations and works for arbitrary molecules. After a short discussion of the mollified impulse method in section 2, we show in section 3 how this new corotational filter can be constructed without using analytical Hessians and Newton iterations. Instead, the new filter can be computed explicitly in a very cheap and effective manner. Furthermore, we prove that the new filter applied to common flexible water models is almost the same as a projection method. In section 4 we introduce four typical simulation scenarios

and discuss the results in section 5. There we provide numerical evidence that the corotational filter is as stable as projection methods, and is, indeed, very computationally efficient.

2. Mollified Impulse Multiple-Timestep Method

In classical molecular dynamics, Hamilton's equations yield atomic trajectories by numerically solving

$$\begin{array}{rl} \dot{q}(t) = & \nabla_p H(q,p) \\ \dot{p}(t) = & -\nabla_q H(q,p) \end{array} \qquad \text{with} \qquad \begin{array}{l} q(t_0) = q_0 \\ p(t_0) = p_0 \end{array} \tag{1}$$

for a given (separable) Hamiltonian function

$$H(q,p) = T(p) + U(q) \quad \text{with} \quad T(p) = \frac{1}{2} p^T M^{-1} p, \tag{2}$$

where we denote atomic positions and momenta by vectors $q(t), p(t) \in \mathbb{R}^{3d}$ at time t, $M \in \mathbb{R}^{3d \times 3d}$ is a diagonal matrix containing the atomic masses, and $U(q)$ represents a potential modeling interaction between atoms.

In this paper we assume that the potential U can be written in the form

$$U(q) = U_{\text{fast}}(q) + U_{\text{medium}}(q) + U_{\text{slow}}(q). \tag{3}$$

Here, the fast intra-molecular part U_{fast} consists of the bond, angle and torsion potentials. The short-range pair interactions U_{medium} are usually modeled with van der Waals and Coulomb potentials within a certain cutoff radius. Finally, we have the remaining long-range electrostatic contributions U_{slow}. Most force-fields for biomolecular simulations admit to such a decomposition [1] - e.g. the AMBER [35], CHARMM [36], GROMOS [37] and OPLS-AA [38] force fields. When numerically computing a trajectory of (1), the impulse method [9, 10] takes advantage of such a decomposition and allows to evaluate faster potentials more often than slower ones.

However, the step size of the impulse method is inherently limited by severe resonances which are caused by an arbitrary evaluation of the slow force at positions which do not represent the oscillatory nature of a molecule [12–15]. Instead, it is advantageous to replace the slow potential U_{slow} in (3) by a mollified version $U_{\text{slow}}(\Psi(q))$ with a filter Ψ. Hence, the slow force $\nabla(U_{\text{slow}}(\Psi(q))) = \Psi_q^T(q) \nabla U_{\text{slow}}(\Psi(q))$ is evaluated at a filtered position $\Psi(q)$ and also post-filtered with the transposed Jacobian $\Psi_q^T(q)$. This is usually referred to as the mollified impulse method [27]. Here, resonances are avoided by first time-averaging the position before evaluating the slow force. Then, the Jacobian removes components of the slow force which would excite the fastest mode, and eventually would lead to resonance issues.

In Algorithm 1, we depict this approach when applied to the potential decomposition in (3). For suitably chosen integers N and K, a step with the mollified impulse method consists of three stages: The inner stage is the application of NK steps of the velocity-Verlet method with step size $h/(NK)$ to the

Algorithm 1: One Step of the Mollified Impulse Method applied to (1) with (2) and (3)

Input: position q, momentum p, step size h, stage factors N, K, filter Ψ
Output: new position q, new momentum p

$p \hookleftarrow p - \frac{h}{2}\Psi_q^T(q)\nabla U_{\text{slow}}(\Psi(q))$
for $i = 1, \ldots, N$ **do**
  $p \hookleftarrow p - \frac{h}{2N}\nabla U_{\text{medium}}(q)$
  for $j = 1 \ldots, K$ **do**
    $p \hookleftarrow p - \frac{h}{2NK}\nabla U_{\text{fast}}(q)$
    $q \hookleftarrow q + \frac{h}{NK}M^{-1}p$
    $p \hookleftarrow p - \frac{h}{2NK}\nabla U_{\text{fast}}(q)$
  $p \hookleftarrow p - \frac{h}{2N}\nabla U_{\text{medium}}(q)$
$p \hookleftarrow p - \frac{h}{2}\Psi_q^T(q)\nabla U_{\text{slow}}(\Psi(q))$

kinetic ($T(p)$) and fast part (U_{fast}) of the Hamiltonian. In the middle stage, at begin and end of every K-th step of the velocity-Verlet method, a half 'kick' with the potential U_{medium} and step size h/N is added. The outer stage only acts at the begin and end of the entire step, and computes a half 'kick' with the slow modified potential $U_{\text{slow}}(\Psi q)$ and step size h. Note, that if we use the trivial 'filter' $\Psi(q) = q$ in Algorithm 1, we obtain the standard impulse method with three stages.

Two types of filters have been proposed in the literature. First, there are filters based on time averaging techniques [15, 32, 33]. Positions are integrated forwards and backwards in time using only the fast forces and then averaged by a weight function Φ:

$$\begin{aligned} &\Psi(q) = \int_{-\infty}^{\infty} \Phi(\tau)x(\tau)d\tau \\ &\text{with} \quad \ddot{x} = -M^{-1}\nabla U_{\text{fast}}(x), \quad x(0) = q,\ \dot{x}(0) = 0. \end{aligned} \tag{4}$$

Second, equilibrium type methods [30, 31] reset the molecule to its equilibrium position using a constraint function g:

$$\begin{aligned} &\Psi(q) = q + M^{-1}g_q(q)^T\lambda, \\ &g(\Psi(q)) = 0. \end{aligned} \tag{5}$$

Note, that for m constraints, $g : \mathbb{R}^{3d} \to \mathbb{R}^m$ is a vector function and $\lambda \in \mathbb{R}^m$ is a vector of Lagrange multipliers. $g_q \in \mathbb{R}^{m\times 3d}$ denotes the Jacobian with respect to the position vector q. Due to the nonlinearity of the problem, (5) is usually solved with a Newton-type method. At a first glance resetting internal degrees of freedom with g might seem too crude of an approximation, but if the outer time-step is large enough this becomes a useful approximation since molecules oscillate around their equilibrium positions.

With these filters, a time-step roughly twice as large compared to a standard multiple time-step method has been achieved. A reliable and stable example is the equilibrium method presented in [30] or a modified version in [31]. Unfortunately, both types of filters need significant computational effort. Averaging filters need to integrate forward and backward (including the derivative!) with the fast forces every outer time-step. Equilibrium methods need to solve nonlinear systems from the constraints.

In the next section, we introduce a new type of filter, which we call *corotational filter*. They are similar to equilibrium filters in the sense, that *corotational filters* also reset certain degrees of freedom within molecules to their equilibrium positions. However, filtered molecules are obtained by an approach based on corotation. While this approach yields a similar quality of the filtering process, it is much cheaper in computational cost. Furthermore, the new filter can be implemented completely without computing trajectory averages or solving nonlinear systems. Instead, it is accessible via a simple and explicit algorithm thus reducing algorithmic complexity in the filtering process.

3. Corotational Filters

The basic idea of corotation is to decompose motion into rotational and translational parts plus deformations from flexibility in bonds and angles. Corotational filters then discard deformational contributions. However, it would be too much to ask, that for an arbitrary molecule, the structure could be well represented by a single rotation. Therefore, we decompose the (potentially very complex) molecular structure into disjunct clusters of much smaller size, e.g. 2-5 atoms.

3.1. Cluster Decomposition of a Biomolecular Structure

The goal of this decomposition is a division of the molecular structure into many but much smaller substructures. Much like in a 'divide and conquer' approach, the substructures are then treated independently, and the connection between substructures is neglected. We call the substructures *clusters*, and every atom should be in exactly one cluster. The construction of the clusters is such that for a fast bond, both atoms need to be part of the same cluster. Only atoms connected by a slower bond are allowed to be members of different clusters. Finally, we require that each cluster has a distinct central atom, which is usually the heaviest one.

Obviously, the classification of faster and slower bonds allows for some choice. Typically, we try to obtain small enough clusters (e.g. 2-5 atoms) such that the overall rotation of that cluster is still a good approximation of the local rotation for all its containing atoms, i.e. that there is no torsional degree of freedom inside a cluster. Of course we could also include trivial clusters containing only a single atom, however, this excludes that atom from the filtering process.

In biomolecular structures, the stretching modes of hydrogen bonds (e.g. H-O, H-N, H-C) are much faster than backbone connections (C-C, C-N, etc).

Thus, most clusters consist of a central atom with fast hydrogen bonds within the cluster, and slower backbone bonds connecting it to other clusters. Let us take an alkane chain as example (see Figure 1). It contains slow backbone bonds (C-C) which connect clusters of methyl (CH_3) and methanediyl (CH_2) groups: CH_3-CH_2-...-CH_2-CH_3. The cluster decomposition yields two terminal clusters of size 4, and then a chain of clusters of size 3.

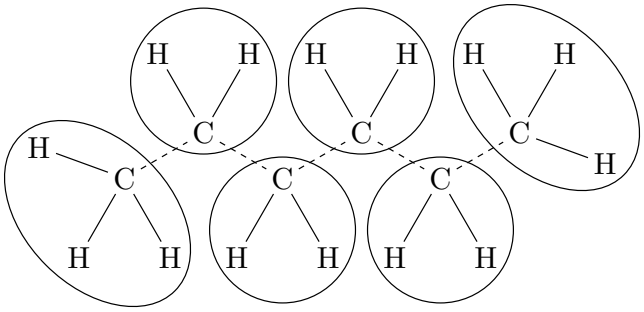

Figure 1: *Cluster Decomposition of Hexane, with two terminal clusters of size 4, and a chain of clusters of size 3. Clusters are indicated by circles, slow bonds are depicted by a dashed line, and fast bonds by a solid line.*

While for simple linear molecules, the choice of clusters is straight forward, it becomes a bit more complex in structures such as aromatic rings. In Figure 2, such a ring structure is decomposed in two different ways. Numerical experiments did not indicate a sensitivity towards the specific decomposition, as long as the fastest bonds were contained inside clusters. Indeed, even very simple decompositions (such as the one used for the peptide in the example section later) yield good results. There are (semi-) automatic algorithms to identify such cluster decompositions, and they are sometimes used in constraining algorithms such as the SHAKE algorithm implemented in LAMMPS [39], since such a decomposition allows for a very efficient implementation.

Similar decomposition approaches are used by many other methods in MD, most notably by coarse-graining methods (see e.g. [40, 41] and references therein) and by internal coordinate molecular dynamics (ICMD) such as the GNEIMO method [42, 43].

3.2. The New Corotational Filter

After generating a cluster decomposition, the clusters are treated independently. We now illustrate the filter algorithm for a single cluster containing n atoms at position $q = [x_1^T, x_2^T, ..., x_n^T]^T \in \mathbb{R}^{3n}$.

A single cluster is a small structure, and can be well represented by its rotational orientation $R \in \mathbb{R}^{3\times3}$ and center of mass $c \in \mathbb{R}^3$. To get rid of internal deformations, we construct a reference position $q_0 \in \mathbb{R}^{3n}$, which has the same structure as this cluster, but with all fast internal degrees of freedom (such as bonds and angles) set back to their corresponding equilibrium values.

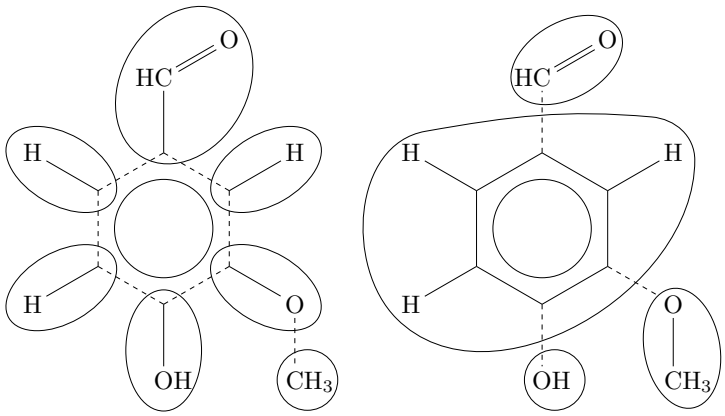

Figure 2: *Two Possible Cluster Decompositions of Vanillin. The first choice decomposes the ring structure with a few small clusters, the second approach uses the entire ring as a cluster, and then cuts off the attached groups. This works, since the aromatic ring can be considered quite stiff.*

This reference configuration is then rotated and shifted to match the cluster's rotation R and center of mass c.

Using Kronecker products $\otimes$, the new corotational filter can be calculated as

$$\Psi(q) = [1, \ldots, 1]^T \otimes c + (I_n \otimes R R_0^T) q_0, \tag{6}$$

where we assume that q_0 has center of mass at $[0, 0, 0]^T$ and rotational orientation R_0. Note, that this can be further simplified, if we choose q_0 such that the resulting R_0 is the identity matrix I_3.

It remains to give an algorithm which quickly approximates the rotational orientation. The given cluster has a central atom with position x_1 bonded to $n-1$ atoms with positions $x_2, ..., x_n$. Let us abbreviate $r_i = x_i - x_1$. A fast way of estimating the rotation between q and q_0 is described in [44]: We compute an orthonormal frame of vectors $R = [n_1, n_2, n_3] \in \mathbb{R}^{3\times 3}$ with

$$\begin{aligned} n_1 &= \sum_{i \in S_1} \frac{r_i}{||r_i||} \Bigg/ \left|\left| \sum_{i \in S_1} \frac{r_i}{||r_i||} \right|\right|, \\ n_2 &= \left(s - s^T n_1 n_1\right) / ||s - s^T n_1 n_1|| \,, \quad s = \sum_{i \in S_2} \frac{r_i}{||r_i||}, \\ n_3 &= (n_1 \times n_2) \,/ ||n_1 \times n_2|| \,, \end{aligned} \tag{7}$$

where we choose $n_1 \in \mathbb{R}^3$ to be an averaged direction of some bonds $i \in S_1$ and for $n_2 \in \mathbb{R}^3$ we choose a different set S_2 of bonds. S_1 and S_2 are suitable chosen, and we illustrate a few common examples in a following section. The vectors n_1, n_2, n_3 form an orthonormal basis of $\mathbb{R}^3$. R_0 is computed in the same way at reference position q_0. Then RR_0^T is an estimate of the rotation from q_0 to q. In Figure 3, we sketch the filter algorithm applied to a cluster of three atoms.

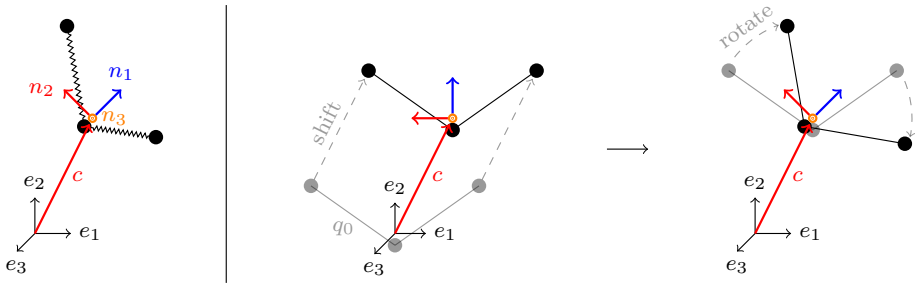

Figure 3: *Illustration of the Corotational Filter Algorithm applied to a cluster with three atoms. First, the center of mass c and rotational orientation n_1, n_2, n_3 are computed. Then, a reference configuration q_0 is shifted and rotated to match the cluster.*

3.3. Properties of the Filter

By construction the filter retains center of mass and rotational orientation of that cluster but by using a reference configuration q_0 internal deformations caused by the fastest oscillations are discarded. Also, if a cluster is already in its equilibrium position q_0, the filter is the identity map, i.e. $\Psi(q_0) = q_0$. Furthermore, the filter is invariant under rotation and translation in the following sense: If R is a rotation, and s is a shift, it holds that $\Psi(Rq + s) = R\Psi(q) + s$.

In (6), the filter depends only on the center of mass and rotational orientation of that cluster. Since the filter is supposed to smoothen the trajectory and remove highly oscillatory components to suppress resonances, the choice of S_1 and S_2 has a strong impact on the success of the filter. While the center of mass of a cluster is independent of fast internal motion, we need to ensure that the choice of S_1 and S_2 leads to a smooth rotational approximation. Constructing R from the direction of the bonds, the fast changes in bond length are already neglected. Furthermore, by a smart combination of neighboring bonds, it is usually possible to remove angle motions. However, not all fast modes can be removed entirely by a linear combination of bond directions, e.g. some asymmetric stretch modes will remain, and we can only reduce the magnitude of those modes. Numerical experiments in section 5 will show though, that this does not pose a problem.

Note, that the filter provides a quite general approach, and there is lots of room for tailoring this filter to one's needs. First, the reference position is computed using the rigid body of that cluster, that is, all internal degrees of freedom are set to their equilibrium values. Since such a reference position does not change over time, it can be precomputed - and that is why we will use this approach in the numerical experiments. But it also works, if only some faster bonds are reset, and e.g. the current angular position is kept. Second, the extraction of rotational information offers some freedom. The more smooth it behaves (under an oscillatory trajectory), the more effective the filter will be. In the given approach, the rotation is estimated using a linear combination of internal directions around a distinct, central atom. But in general, any other

approach which gives a robust estimation can be used.

3.4. Examples of Sizes 2-4

The filter presented in the compact notation in (6) and (7) is not very instructive. Here, we present examples for cluster sizes $n = 2, 3$ and 4. For $n = 2$ and 3, the filter can be expressed more succinctly.

In the simple case $n = 2$, two atoms x_1, x_2 with masses m_1, m_2 are connected via a single bond with equilibrium length r_0. Because of its symmetries, the cluster can be described by a single direction, i.e q_0 has no contribution in direction of n_2, n_3. We choose

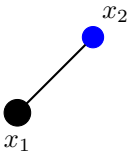

$$n_1 = \frac{x_2 - x_1}{||x_2 - x_1||},$$
$$n_2,\ n_3 \ \text{ s.t. they form an orthonormal basis.}$$

Therefore, the filter reads

$$\Psi(q) = \begin{pmatrix} c + a_1 n_1 \\ c + a_2 n_1 \end{pmatrix}, \qquad \text{with} \quad \begin{aligned} a_1 &= -\frac{m_2}{m_1 + m_2} r_0, \\ a_2 &= \frac{m_1}{m_1 + m_2} r_0. \end{aligned} \tag{8}$$

In the formalism of (6) and (7) this corresponds to $S_1 = \{2\}$ (since it only uses the bond $r_2 = x_2 - x_1$).

For a triatomic cluster ($n = 3$), we can reduce by one dimension if we choose the reference cluster $q_0 \in \mathbb{R}^9$ in the (x, y)-plane. Since the z-component is zero, we can omit the computation of n_3. We consider the following choice:

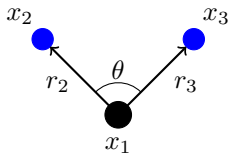

$$\begin{aligned} n_1 &= \left(\frac{r_2}{||r_2||} + \frac{r_3}{||r_3||} \right) \Big/ \left|\left| \frac{r_2}{||r_2||} + \frac{r_3}{||r_3||} \right|\right|, \\ n_2 &= \left(r_2 - r_2^T n_1 n_1 \right) / ||r_2 - r_2^T n_1 n_1||. \end{aligned} \tag{9}$$

This particular choice ($S_1 = \{2, 3\}, S_2 = \{2\}$) has the advantage that vibrations due to angle bending and symmetric bond stretching are entirely removed by design; if r_2 changes as much in an opposite direction as r_3, then there is no influence on n_1. n_2 does not change either since r_2 stays in the same plane. This property holds for any triatomic symmetric molecule, most notably for flexible water models.

The filter then reads (q_0^i denotes the i-th entry of q_0)

$$\Psi(q) = \begin{pmatrix} c + q_0^1 n_1 + q_0^2 n_2 \\ c + q_0^4 n_1 + q_0^5 n_2 \\ c + q_0^7 n_1 + q_0^8 n_2 \end{pmatrix}. \tag{10}$$

However, we have to make one restriction: If θ is close or equal to 180° such as in thiocyanate (SCN) or hydrogen cyanide (HCN), $r_2/||r_2|| + r_3/||r_3||$

threatens to cancel. Thus, for such a cluster, it is much better to use a treatment similar to the case $n = 2$ with

$$n_1 = \left(\frac{r_2}{||r_2||} - \frac{r_3}{||r_3||} \right) \Big/ \left|\left| \frac{r_2}{||r_2||} - \frac{r_3}{||r_3||} \right|\right| . \tag{11}$$

Clusters with four atoms ($n = 4$) frequently happen with terminal CH_3 groups, where the carbon atom has a slow bond connecting it onwards to the next cluster.

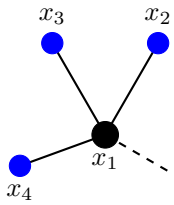

Here, the best choice would be $S_1 = \{2, 3, 4\}$. For S_2 we choose any two of the 'satellites': $S_2 = \{2, 3\}$ or $S_2 = \{3, 4\}$ or $S_2 = \{2, 4\}$. However, in a planar tetra-atomic structure (such as formaldehyde H_2CO) similar to the three atomic linear case we face the danger that $r_2 + r_3 + r_4 \approx 0$. Instead, we then choose S_1 and S_2 such that n_1, n_2 reliably characterize the plane in which the cluster lives.

We want to finish by pointing out one detail for the simulation of flexible water. For flexible water, we can directly compare the existing equilibrium filter from [30] to our new filter. The equilibrium filter is given by (5) with

$$g(q) = \begin{pmatrix} ||x_2 - x_1||^2 - r_0^2 \\ ||x_3 - x_1||^2 - r_0^2 \\ ||x_3 - x_2||^2 - 2r_0^2(1 - \cos\theta_0) \end{pmatrix}$$

for water molecules at position $x_1(\text{oxygen}), x_2, x_3 \in \mathbb{R}^3$ with equilibrium bond length r_0 and equilibrium angle θ_0. Hence for every molecule a small 3-by-3 nonlinear constraint system has to be solved e.g. with a simplified Newton method. Since the molecules are close enough to an equilibrium position, this method usually converges within a few steps. Nevertheless, it is more expensive than the corotational filter since the latter only costs roughly as much as a single Newton step.

Now, the interesting point is, that for water molecules (or any symmetric triatomic molecules) equilibrium (5) and corotational filter (6) with (9) are close in the sense that they are exactly equal whenever the two bonds have equal length.

This is quite straight forward to show, since a water molecule in its equilibrium position is uniquely identified by its center of mass and rotation matrix R containing the vectors $n_i, i = 1, 2, 3$. Both filters maintain center of mass. For the corotational filter (by design) the vectors n_i do not change during filtering. So we only need to check the vectors n_i for the equilibrium filter.

It is, in fact, sufficient to check n_1 since both filters do not alter the plane in which the molecule lives. Denoting filtered values with tilde, easy calculations reveal that after filtering we have

$$\frac{\tilde{r}_1}{||\tilde{r}_1||} + \frac{\tilde{r}_2}{||\tilde{r}_2||} = \frac{r_1}{r_0}\left(1 + \frac{\lambda_1}{m_2} + 2\frac{\lambda_1}{m_1}\right) + \frac{r_2}{r_0}\left(1 + \frac{\lambda_2}{m_3} + 2\frac{\lambda_2}{m_1}\right)$$

where m_i is the mass associated with x_i. If we would have $m_2 = m_3$ and $\lambda_1 = \lambda_2$ then we would have

$$\frac{\tilde{r}_1}{||\tilde{r}_1||} + \frac{\tilde{r}_2}{||\tilde{r}_2||} = c\left(\frac{r_1}{||r_1||} + \frac{r_2}{||r_2||}\right), \quad c \in \mathbb{R}$$

and hence n_1 would not change during filtering for the equilibrium method.

Obviously for water we have $m_2 = m_3$. Furthermore, by assumption, both bonds have the same length and there is a solution with $\lambda_1 = \lambda_2$. Since $\frac{\partial g(\Psi(q))}{\partial \lambda}$ has full rank, this solution is also unique by the implicit function theorem.

3.5. The Jacobian of the Corotational Filter

Application within the mollified impulse method requires the Jacobian $\Psi_q(q)$. In contrast to other filters in the literature, the derivative of the corotational filter is explicitly given and easy to compute. It does not require the solution of any nonlinear systems. Note, that both filter and its derivative are spatially local properties, making a parallel implementation within a domain decomposition strategy fairly easy.

With notation as in 6 and 7 for a cluster of n atoms we have

$$\Psi(q) = [1, .., 1]^T \otimes c + (I_n \otimes RR_0^T)q_0$$

with

$$\begin{aligned}
n_1 &= \sum_{i \in S_1} \frac{r_i}{||r_i||} \Bigg/ \left|\left| \sum_{i \in S_1} \frac{r_i}{||r_i||} \right|\right| =: \frac{u}{||u||}, \\
n_2 &= \left(s - s^T n_1 n_1\right) / ||s - s^T n_1 n_1|| =: \frac{v}{||v||}, \\
n_3 &= (n_1 \times n_2) / ||n_1 \times n_2|| =: \frac{w}{||w||}.
\end{aligned}$$

We choose the reference cluster $q_0 = [q_0^1, q_0^2, \ldots, q_0^{3n}]^T \in \mathbb{R}^{3n}$ such that R_0 is the identity I_3. The derivative then simplifies to:

$$\Psi_q(q) = [1, ..., 1]^T \otimes \frac{\partial}{\partial q} c + \begin{pmatrix} q_0^1 \frac{\partial n_1}{\partial q} + q_0^2 \frac{\partial n_2}{\partial q} + q_0^3 \frac{\partial n_3}{\partial q} \\ q_0^4 \frac{\partial n_1}{\partial q} + q_0^5 \frac{\partial n_2}{\partial q} + q_0^6 \frac{\partial n_3}{\partial q} \\ \ldots \end{pmatrix} \tag{12}$$

with

$$\begin{aligned}
\frac{\partial n_1}{\partial q} &= \frac{1}{||u||}\left(I_3 - n_1 n_1^T\right)\left(\sum_{i \in S1} \frac{1}{||r_i||}\left(I_3 - \frac{r_i}{||r_i||}\frac{r_i^T}{||r_i||}\right)\frac{\partial r_i}{\partial q}\right), \\
\frac{\partial n_2}{\partial q} &= \frac{1}{||v||}\left(I_3 - n_2 n_2^T\right)\left[\left(I_3 - n_1 n_1^T\right)\frac{\partial s}{\partial q} - \left(s^T n_1 I_3 + n_1 s^T\right)\frac{\partial n_1}{\partial q}\right], \\
\frac{\partial n_3}{\partial q} &= \frac{1}{||w||}\left(I_3 - n_3 n_3^T\right)\left(\frac{\partial n_1}{\partial q} \times n_2 + n_1 \times \frac{\partial n_2}{\partial q}\right).
\end{aligned} \tag{13}$$

The derivative of the center of mass in (12) is given by

$$\frac{\partial c}{\partial q} = \frac{1}{m_{\text{all}}}[m_1, m_2, \ldots, m_n] \otimes I_3, \qquad \text{with} \qquad m_{\text{all}} = \sum_{i=1}^{n} m_i. \tag{14}$$

Note, that in (13) we have $\partial r_i/\partial q = (e_i - e_1) \otimes I_3$ where e_k denotes the k-th canonical unit vector. Furthermore,

$$\frac{\partial s}{\partial q} = \sum_{i \in S2} \frac{1}{||r_i||} \left(I_3 - \frac{r_i}{||r_i||} \frac{r_i^T}{||r_i||} \right) \frac{\partial r_i}{\partial q} \tag{15}$$

and a similar expression but for S_1 already appears in $\partial n_1/\partial q$. Thus, if there is an overlap between S_1 and S_2, we can reuse part of that calculation. In the last row of (13) we slightly abuse the notation, and the cross products are meant column-wise. The derivative looks quite nasty, but one is reminded, that most quantities are constructed from simple vectors of size 3, which already have been computed with the filter. Also, from an implementational viewpoint, the matrix Ψ_q does not need to be constructed explicitly, instead only its action on the force vector is required.

For the cases $n = 2, 3$ the derivative can be expressed much shorter. In the setting of (8), for a cluster with two atoms the derivative reads

$$\begin{aligned} \Psi_q(q) &= [1, 1]^T \otimes \frac{\partial}{\partial q} c + \begin{pmatrix} a_1 \frac{\partial n_1}{\partial q} \\ a_2 \frac{\partial n_1}{\partial q} \end{pmatrix}, \\ \frac{\partial n_1}{\partial q} &= \frac{1}{||x_2 - x_1||} (I_3 - n_1 n_1^T)[-I_3, I_3]. \end{aligned} \tag{16}$$

The derivative for a cluster with three atoms as obtained from (10) is

$$\Psi_q(q) = [1, 1, 1]^T \otimes \frac{\partial}{\partial q} c + \begin{pmatrix} q_0^1 \frac{\partial n_1}{\partial q} + q_0^2 \frac{\partial n_2}{\partial q} \\ q_0^4 \frac{\partial n_1}{\partial q} + q_0^5 \frac{\partial n_2}{\partial q} \\ q_0^7 \frac{\partial n_1}{\partial q} + q_0^8 \frac{\partial n_2}{\partial q} \end{pmatrix}. \tag{17}$$

3.6. The Full Algorithm

Algorithm 2 summarizes the necessary steps as explained in the previous sections. First, a cluster decomposition of the molecular structure has to be determined and the individual reference configurations for each cluster need to be computed. Since both the cluster decomposition and the reference configurations only need to be computed once for every structure, they can be precomputed.

Now, whenever we need the filtered position and its derivative, for each cluster, we estimate the local rotation. By rotating and shifting the corresponding reference configuration we obtain the filtered position for each cluster. This way internal deformations, which are not represented by overall rotation or center of mass movement of a cluster, are discarded. The filtered position of the entire molecular system then is assembled by simply taking the filtered values from each individual cluster. In a similar manner, we proceed with the Jacobian of the filter.

Algorithm 2: Corotational Filter Algorithm

Input: position q
Output: filtered position $\Psi(q)$, Jacobian $\Psi_q(q)$
Precompute:
- generate a cluster decomposition
- compute a reference configuration for each cluster
Filter:
for *each cluster* **do**
  - estimate local rotation via (7)
  - compute filtered position via (6)
  - compute Jacobian via (12)

-assemble $\Psi(q), \Psi_q(q)$ from individual clusters

4. Test Problems

We test the corotational filter's stability and performance on four different problems. First, in problem (A) we choose the most common natural form of ice, that is ice Ih. Ice is very sensitive to changes and its structure is easily destroyed by a misperforming integrator. This makes it an outstanding test problem. As second problem (B) we choose a small peptide solvated in explicit water. It has a huge variety of vibrations from bonds, angles and torsions. It also shows that it is possible to find a suitable choice of clusters. In simulation (C) we investigate ice-ice friction, and in simulation (D) folding phenomena of a protein are investigated. In contrast to the more academic test problems (A) and (B), the dynamics of problems (C) and (D) are much more complex and interesting. They also indicate that the proposed filtering technique is reliable and stable in application.

These models pose excellent testing problems since expensive long-range forces have to be computed every time-step. However, high oscillations due to bond stretching and angle bending limit the step size of the (unfiltered) impulse method to below 4fs. They also show that the new filter can easily handle different potential structures. In fact, the filter will work with all flexible molecules regardless of their potential structures. We only have to find a cluster decomposition and identify suitable equilibrium positions for the filter to work.

4.1. Problem (A) for Ice Ih

Ice Ih has a hexagonal lattice structure (see [45] for lattice parameters). We set up a cubic simulation box with periodic boundaries containing 2880 molecules. The simulation size is sufficiently large to get reliable results and obtain a computationally challenging problem (parallel efficiency is a major concern).

There are many atomistic models for water, each with different properties and each is optimized for some special purpose. For a good overview see, for example, [46]. We conduct our investigation by choosing two different flexible

models. First we choose the SPC/F model [47], which is based on the rigid three site SPC model and uses harmonic potentials in bonds and angles to model intra-molecular forces. The second model we investigate is TIP4P/2005f [48], a flexible model based on the TIPNP topology. It additionally uses a massless fourth site, M, with a negative charge. Bond interactions are modeled using a Morse potential. The angle potential is again harmonic.

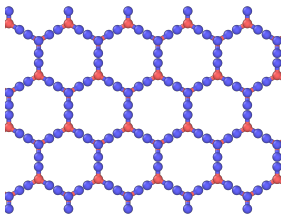

Figure 4: *Ice Ih in its perfect crystal lattice structure, crop of simulation cell.*

For water, the cluster decomposition is natural: Each molecule is a cluster of size three. The reference configurations then is simply a water molecule with equilibrium bond length and angle as specified in the corresponding water model.

4.2. Problem (B) for a Small Peptide

We conduct simulations of a small 5-mer peptide solvated in water. Initial positions and structure can be found in the LAMMPS example section. The peptide has 84 atoms and is solvated in 640 water molecules (total of 2004 atoms). Potentials are modeled according to the CHARMM forcefield [49]. For the cluster decomposition each water molecule forms its own cluster. The decomposition of the peptide is chosen such that all bonds containing a hydrogen and carbonyl groups (C=O) are filtered. Then, the peptide decomposes in clusters mostly of size two and three. However, there are three terminal CH_3 groups which form clusters of size four, and four single atoms remain, that we choose not to filter. Of the four unfiltered atoms, three are carbon atoms with slow onwards connections in the aromatic rings, and the last one is a sulfur atom connected with two slow bonds to a CH_3 and CH_2 group. Note, that those four atoms can be easily included in a neighboring cluster, however, as the numerical results indicate, due to their slow bonds, this is not necessary. In total, the decomposition has 25 clusters of size 2, 646 of size 3 and 3 of size 4.

4.3. Problem (C) for Ice-Ice Friction

The third test problem investigates friction processes between two layers of ice Ih. It has been known for a long time that the creation of a liquid layer in between the ice interfaces plays a significant role. The investigation of the dynamics and mechanisms in this liquid layer is an active area of research from both theoretical/computational and experimental groups [50–54].

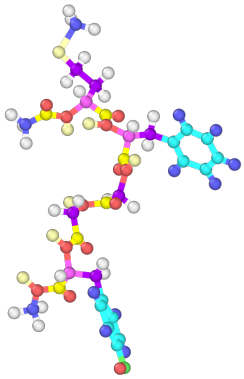

Figure 5: *A small peptide, depicted in its ball-stick representation. For simulation (B) it is solvated in 640 water molecules.*

Similar to [52], we create two slabs of ice separated by some vacuum in z-direction and bring them slowly into contact. The motion of the two slabs is controlled by harmonically restricting the movement of a layer of water molecules in each slab (indicated by yellow coloring in Figure 6). This allows us to control friction velocity and contact pressure.

Each slab contains 2880 molecules, in total we have to keep track of 17280 atoms. We choose the TIP4P/2005f model for this investigation. Computationally this is also a very challenging problem, especially if we are interested in slow friction velocities.

4.4. Problem (D) for Bovine Pancreatic Trypsin Inhibitor

Bovine pancreatic trypsin inhibitor (BPTI) is a small protein which can be found in bovine lung tissue. Its function is suppression of protein digestion and it acts as a competitive inhibitor. For example during heart surgery it can be used to reduce bleeding. Well studied since the 70s/80s, it exhibits complex folding pathways.

Structural information was obtained from the RCSB database (ID: 4PTI[55]). BPTI has 892 atoms, and we solvate it in 3165 explicit water molecules (10387 atoms in total). Potentials are modeled according to the CHARMM forcefield [49]. For the filter decomposition, we use the simple heuristic, that bonds containing a hydrogen are fast bonds, and the remaining ones are slow. Thus, we obtain 163 clusters of size 2, 3263 of 3 and 25 of 4.

4.5. Time Integration

We investigate three variations of the impulse method with different settings and the Verlet method:

Impulse Method (IM): The unfiltered standard impulse method uses three stages with the force splitting described in (3). This corresponds to Algorithm 1 with the trivial filter $\Psi(q) = q$, so the force kick in the outer stage

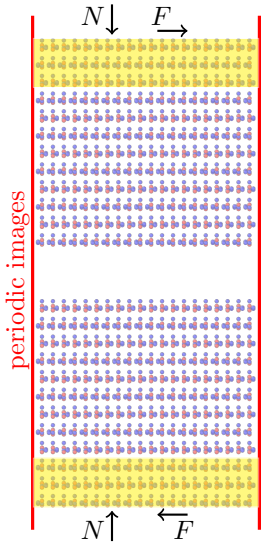

Figure 6: *Ice Friction Model for Problem (C) as defined in Section 4.3: two slabs of ice will be brought into contact by applying normal and friction force by harmonically restricting the molecules in yellow indicated areas. Red lines indicate periodic box boundaries.*

reads

$$p \hookleftarrow p - \frac{h}{2}\nabla U_{\text{slow}}(q). \tag{18}$$

The stage factors N, K control the step sizes of the different stages: While the outer stage uses step size h, the middle stage updates with h/N and the inner stage with h/NK. Therefore, step sizes of inner and middle stages varied depending on the outer step size. We chose N, K such that the middle stage (pair forces) use the closest step size smaller than or equal to 1fs, and the inner stage (bonded forces) use the closest one smaller than or equal to 0.5fs, i.e. $N = \lceil h \rceil, K = 2$.

Corotational Mollified Impulse Method (CIM): Same as the IM but the outer stage is now equipped with the new corotational filter (6) introduced in Section 3.

Equilibrium Mollified Impulse Method (EIM): Same as the IM and CIM but the outer stage uses the equilibrium filter in (5) for water.

Verlet method: Standard velocity-Verlet algorithm used for reference purposes.

4.6. Implementation

We use LAMMPS to perform molecular simulations. The necessary force fields and methods for long-range electrostatic contributions are already implemented. The extensions to run simulations in NPT/NVT ensembles use Nose-Hoover thermostats. For analysis of output data we use VMD [56], Ovito [57] and our own scripts.

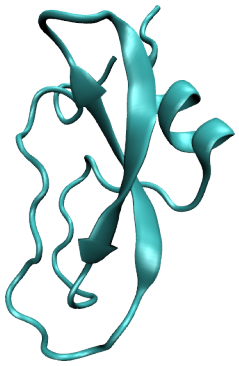

Figure 7: *BPTI with its secondary structure for Test Problem (D) defined in Section 4.4*

Both the Verlet method and the IM are already available in LAMMPS. We implement the new corotational filter and equilibrium filter in LAMMPS using pre- and post-force routines. In especially, the pre-force part consists in computing the filtered position and the filter's derivative. When the slow force has been computed, the post-force part applies the derivative to the slow force.

5. Results

5.1. Simulations of Small Test Problems (A) and (B)

5.1.1. Vibration Reduction using the Corotational Filter

In order to avoid resonances in the mollified impulse method, the corotational filter is designed to eliminate fast vibrations in the position of molecules. After equilibration (A: 50ps, NPT with 150°K and 1bar pressure, B: 50ps, NVT with 250°K), we extract trajectories of a selection of molecules for 10ps (IM with 1fs outer step size) and use VMDs IR analysis tool to compute vibrational spectra. Then we apply the corotated filter algorithm (6) directly to each time-step of the extracted trajectories and repeat the analysis. Note that differences in peak heights stem from normalizing.

In Figure 8 we clearly see how filtering entirely removes frequencies associated with the highest frequencies. There are tiny artifacts remaining though: for example asymmetric bond stretching in the SPC/F model creates a contribution which is barely visible and has drastically reduced amplitude (by more than two orders of magnitude). We do not believe this to be a problem, since the slow force contributions exciting the asymmetric bond stretching modes are filtered out by the derivative. The filter does not seem to influence any other frequencies, the peaks are in exactly the same positions.

Note that in both CIM and EIM, the filtered positions are only used to evaluate the slow forces, hence both integrators (in contrast to SHAKE) still resolve fast bond and angle vibrations.

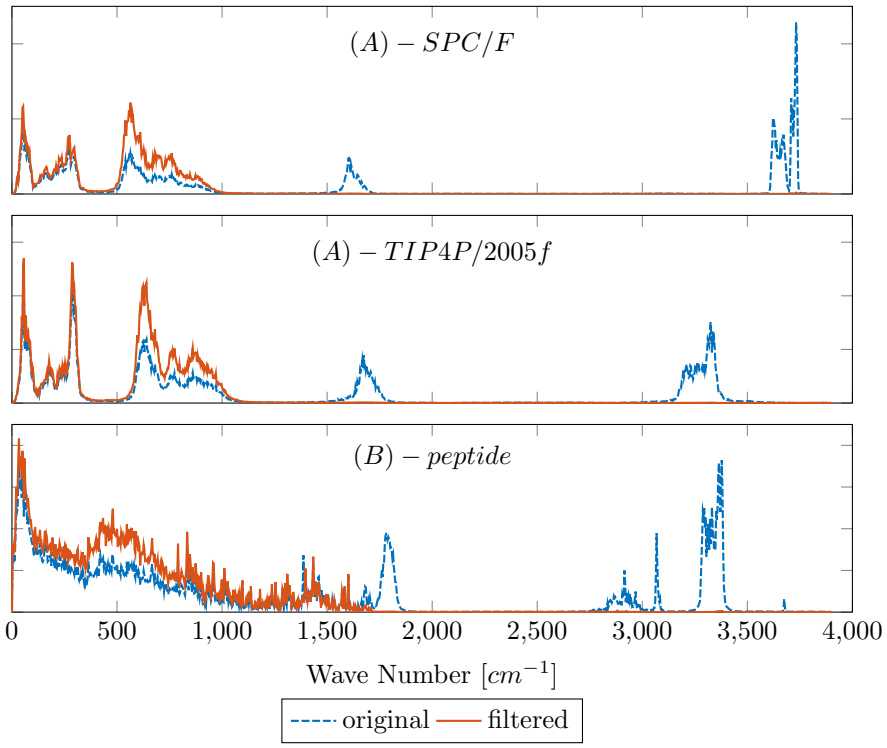

Figure 8: *Infrared spectra obtained for Problems (A) and (B) from 10ps trajectories: wave number* $[cm^{-1}]$ *vs intensity*

5.1.2. Energy Drift

Geometric integrators [58] have the ability to approximately preserve energy. Hence the energy drift with respect to step size is a property of interest. After equilibration (A: 50ps, NPT with 150°K and 1bar pressure, B: 50ps, NVT with 250°K) we run 50ps NVE simulations with IM, CIM and EIM. Since the energy is slightly oscillating we choose to average over the first and last 500fs to cancel out oscillations and approximate drift. For filtered versions we compute the energy at the filtered slow potential $U_{\text{slow}}(\Psi(q))$.

Figure 9 indicates that for ice simulations with the SPC/F model, the impulse method can easily handle outer step sizes as big as 4fs without significant drift. Resonance issues cause, as expected, a dramatic breakdown at step sizes near 4.5fs. It is a 2:1 resonance failure attributed to the fast bond oscillations. Due to a clear separation of frequency bands, it is a sharp spike. With larger time-steps we can get stable results again. Note that at time-steps between 4.4 and 4.6fs the simulation actually 'explodes' and therefore aborts half way through. Furthermore, we can also detect nonlinear resonances other than the critical 2:1 breakdown. Following [14] we expect 3:1 and 4:1 instabilities, which happen not at half the period, but at a third or a fourth of the associated mode.

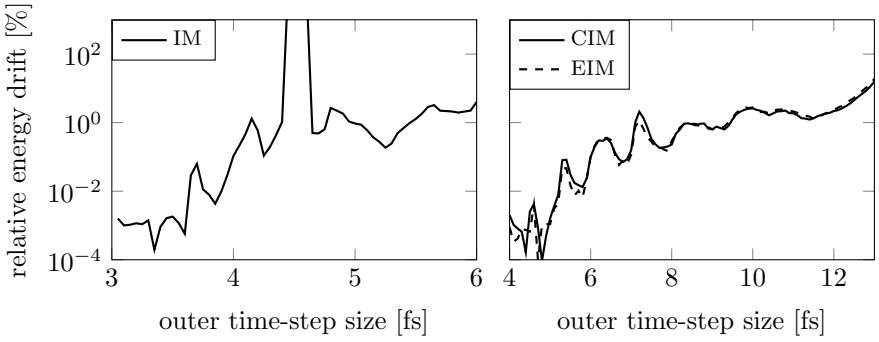

Figure 9: *Problem (A) with the SPC/F model: relative energy drift [%] vs outer time-step size [fs]*

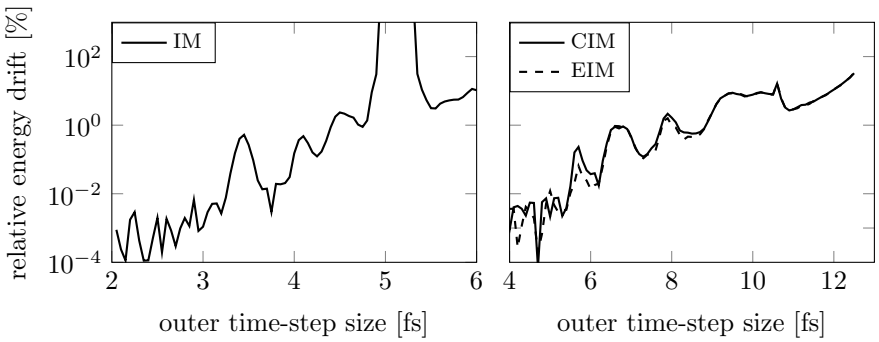

Figure 10: *Problem (A) with the TIP4P/2005f model: relative energy drift [%] vs outer time-step size [fs]*

The peaks in energy drift at around 3.7fs and 4.2fs might stem from such higher order resonances, resulting from the angular motion. The situation is found to be similar for the TIP4P/2005f. For this case, the 2:1 instabilities occur near 5fs (see Figure 10). The peak at 3.4fs is clearly a 3:1 instability, and the smaller peaks at 4.1fs and 4.6fs could be originated in higher order resonances, resulting from the angular motion. Due to the multitude of different frequencies in the motion of the peptide in (B), it is much harder to assign resonances. In Figure 11 it is clear, though, that the first dramatic breakdown happens around 5fs. Other resonances are more smeared and difficult to identify, but clearly visible.

Severe resonance instabilities as observed with the unfiltered IM do not seem to appear in the filtered integrators at all. In fact, step sizes as large as 10 fs (or around 9fs for the TIP4P model) can be used if we are willing to accept a drift of less than 1% on a 50ps run with 2880 molecules. This should not be a problem if we are running very long simulations within a NVT/NPT ensemble with a very weak coupling to a target temperature and/or pressure. As for the

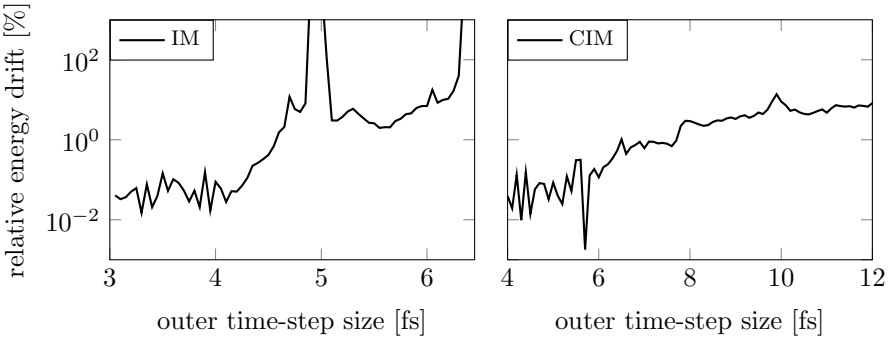

Figure 11: *Problem (B) with the peptide: relative energy drift [%] vs outer time-step size [fs]*

impulse method, there are artifacts of nonlinear resonances visible for both CIM and EIM. We suspect that they originate from modes associated with angle vibrations at around 20.8fs (SPC/F) and 20.2fs (TIP4P/2005f). The peaks around 10fs are then 2:1 instabilities, those just below 7fs are 3:1 resonances, and the remaining peaks are probably a mix of 3:1 and 4:1 resonances from different modes. These results clearly show the improved performance of the proposed filters against existing integrators.

5.1.3. Energy Distribution

Filtering long-range force contributions successfully removes resonance instabilities which originate from the fastest vibrations. However, filtering interferes with the slow energy exchange between fast and slow modes e.g. as shown theoretically for the Fermi-Pasta-Ulam problem in [58], chap. XIII and references therein. We compare differences in the potential energy of U_{fast}, U_{medium} and U_{slow}. After 250ps equilibration (A: NPT at 180°K and 1bar, B: NPT at 250°K and 1bar) with each method we collect these values for 10ps. Figure 12 plots the relative difference $\Delta U = |U_{\text{CIM}} - U_{\text{IM}}|/|U_{\text{IM}}|$, where we use the CIM with an 8fs outer time-step and the IM as a reference solution with outer time-step of 1fs.

These plots indicate that there is a slight difference, primarily in bonded interactions. This is somewhat expected since we mollify the long-range force contributions exactly in the direction of these interactions. We further investigate the impact of filtering and analyze the radial distribution functions.

5.1.4. Radial Distribution Function

A radial distribution function (RDF) is a structural fingerprint. Here we investigate the RDF between oxygen atoms obtained after 250ps equilibration in NPT at 180°K and 1bar with each method.

In Figure 13 we compare RDFs obtained with a large step CIM at 8fs to a reference solution using the IM with a small outer step size of 1fs. Bond and pair forces are computed every 0.25fs. The data is collected and averaged over 10ps.

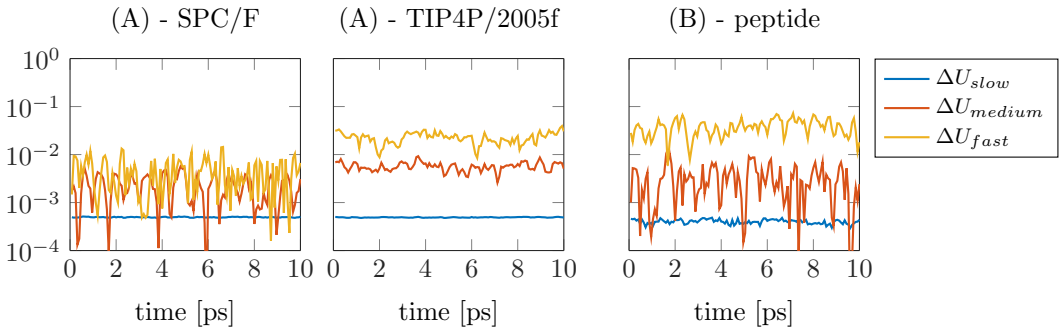

Figure 12: *For Problems (A) and (B) the relative energy difference vs time for the CIM is plotted*

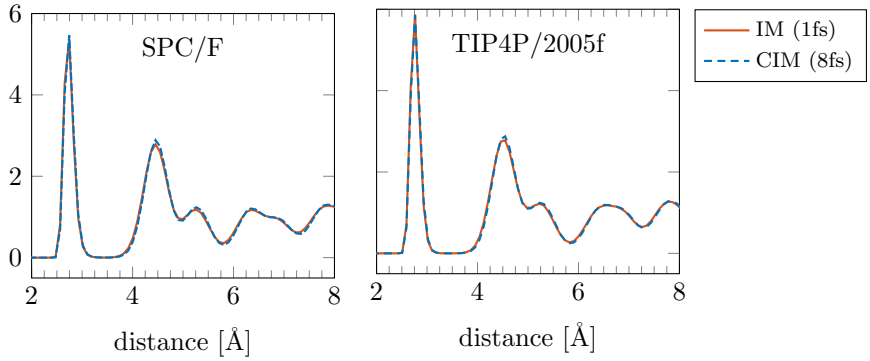

Figure 13: *For Problem (A): RDFs of oxygen-oxygen distribution for the SPC/F and TIP4P/2005f model*

The results are almost indistinguishable, and we have peaks at exactly the same positions. There are small differences in height for the two models, with a slight emphasis on the low energy positions for the proposed filter. However, these discrepancies are so little that they can be safely neglected in most applications. Investigating both the energy distribution and the RDFs, we have no indication that filtering overly manipulates the energy flow.

5.1.5. Computational Cost

Computational and implementational efficiency are the main motivations behind design and construction of our new filter. It should be noted that timing information is not only extremely hardware sensitive, but also strongly depends on problem size and implementation. We give results for problem (A), and the other problems are expected to behave in a very similar way.

The cost of the long-range electrostatic forces plays a major role; the more expensive they are the more we can gain by using new filters developed here. As our previous results indicate, the CIM can easily use an outer step size which is twice as large. This means it only evaluates the slow force half as often compared

to a regular IM with a 4fs step size. In case the slow force is computationally cheap, we can shift the cutoff radius so that a bigger portion of the force is computed in the outer stage. Also, using a GPU can significantly decrease the pair time [59].

Timing results in Figure 14 are obtained from short 50ps simulations after equilibration. The results are averaged over ten runs each. They are obtained on the bwUniCluster (see Acknowledgments) using 128 cores (8 nodes with 16 cores each). Categories are as follows: *'Bond'* contains the computation of

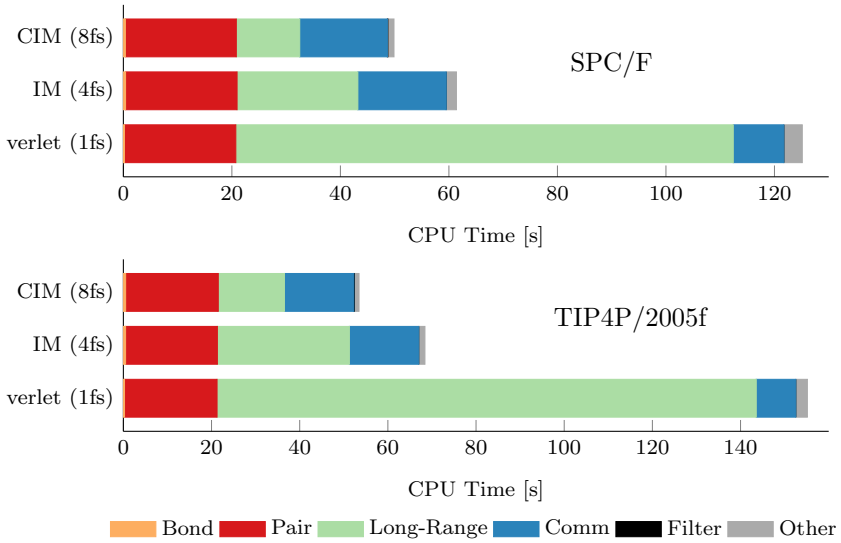

Figure 14: *Absolute CPU time in seconds walltime for Problem (A) and the SPC/F and TIP4P/2005f model, as obtained from short 50ps simulations using 128 cores. For the CIM, the time spent on the filter is below 0.1s for both models.*

intra-molecular forces, *'Pair'* the time spent on evaluating all forces between molecules within a certain cutoff. *'Long-Range'* is the time used calculating the long-range electrostatic contributions. *'Comm'* represents all time due to communication between processors. *'Filter'* signifies all computations assigned to the pre- and post-filtering. Remaining time is summarized in *'Other'*.

The improvement of CIM over a regular Verlet method is about eight times less time spent on long-range computations. Compared to a standard IM, the CIM saves half the computational cost of long-range interactions. The additional computation of the filter itself is very cheap and costs less than 0.1% overall CPU time. Therefore, in Figure 14, it is represented by a very narrow black line between *Comm* and *Other*. Obviously, we also timed the EIM, but do not give separate results. Qualitatively, it is the same as the CIM, and only differs in the filtering time, where it tends to be 50% more expensive. However, the overall variation between the ten runs each is of a similar magnitude.

In general at least $15-20\%$ overall speed up can be expected by using the filtered CIM compared to a standard IM; and $>50\%$ gains over the traditional

Verlet algorithms can be accomplished.

5.2. Simulation of Ice-Friction in Problem (C)

The following simulations are computed with the CIM, using an outer step size of 8fs. The gain in computational efficiency makes it possible to investigate slower friction velocities and compute longer trajectories. First, we investigate ice friction between two slabs of ice Ih with the TIP4P/2005f model.

5.2.1. Simulation Protocol

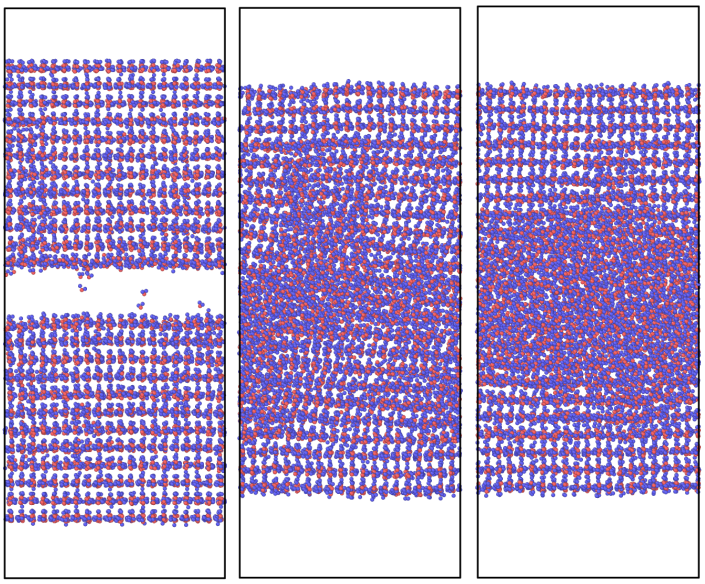

Figure 15: *Snapshots after 800ps, 1200ps and 9200ps, 5m/s friction velocity for Problem (C)*

For equilibration we perform 800ps in NPT targeting 1.0bar and slowly heating up to 180°K. After equilibration, the simulation runs in NVE except for the constrained layers, where temperature is controlled by a Nose-Hoover thermostat. Throughout the process, friction causes heat to be generated at the interface. Hence with temperature control of constrained layers, we model heat dissipation out of the domain.

Then each slab is set to an opposing velocity and we start applying a normal force to the constrained layers of molecules. We run for another 8.4ns where we slowly increase the target temperature of the constrained layers to 210°K. Afterwards, we keep the temperature of the constrained layers fixed at 210°K and run for another 8ns.

The friction velocity is chosen ranging from 0.01m/s to 10m/s. For the imposed normal force we select 10 and 100kcal/mol-Å, half of each is applied to the top layer, the other half is applied in the opposite direction to the bottom layer.

5.2.2. Friction Force

Previous experimental studies [53, 54] found that friction forces are rather sensitive to a variety of parameters such as velocity, normal force and temperature. Unfortunately, it takes a long simulation to get from static friction to kinetic friction. Figure 16 shows one simulation run, plotting the average friction force over time (at 100kcal/mol-Å normal force and 5m/s velocity). We can see that as soon as the slabs come into contact, due to static friction, there is a high peak in friction. The strong connections subsequently begin to break down, and we observe sliding between the layers. The force of friction drops quickly in the beginning, but much slower afterwards. It takes a long time to converge.

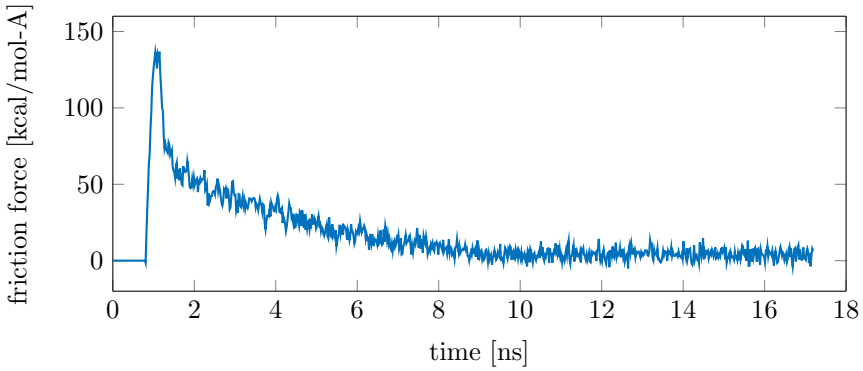

Figure 16: *Averaged friction force [kcal/mol-Å] vs time [ns], at 5m/s, 100 kcal/mol-Å normal force for the Problem (C)*

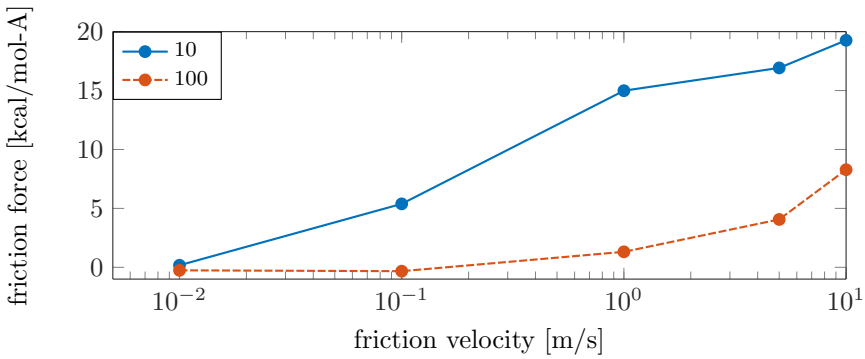

Figure 17: *Average final friction force for 10 and 100 kcal/mol-Å normal force and different friction velocities, friction force [kcal/mol-Å] vs friction velocity [m/s] for Problem (C)*

Results obtained by varying velocity and normal force are plotted in Figure 17. Force values are averaged over the last 4ns of the 17.2ns runs. They

seem to indicate two relations: first, the higher the velocity, the larger the friction, and second, higher normal force, as compared to lower normal force, is correlated with significantly lower friction.

5.2.3. Temperature Distribution and Liquid Layer

In the simulation, friction generates heat and temperature increases around the interface. A liquid layer is formed at the interface which has an increased density. In [60], an order parameter as indicator for the structure of ice Ih is introduced. It would be 1 in a perfect tetrahedral network, or 0 in an ideal gas. As noted in [52], in practice we can expect it to be around 0.95 in ice, and around 0.5 to 0.85 in liquid water.

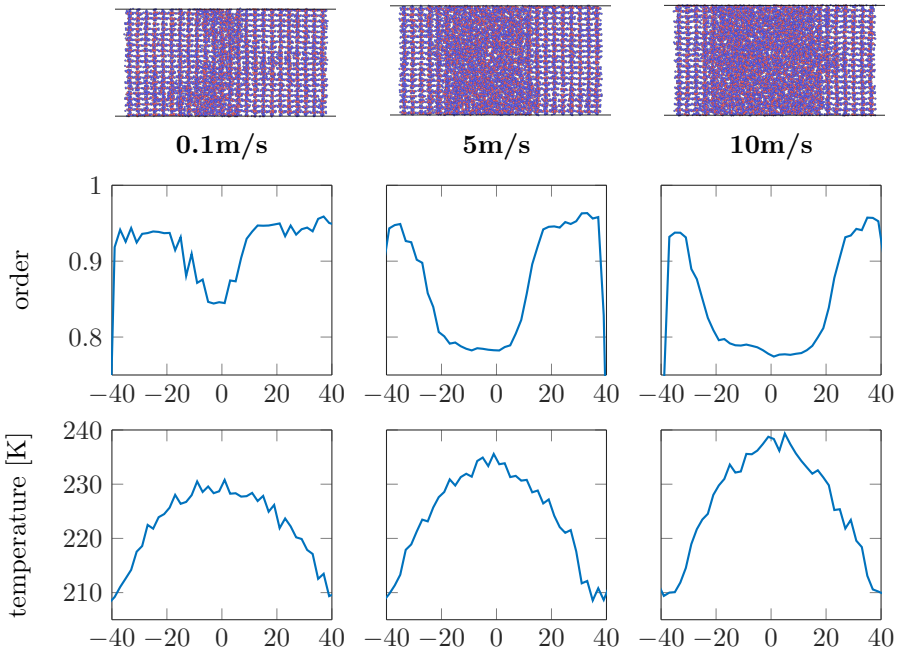

Figure 18: *The thickness of melted layer at 10 kcal/mol-Å for different friction velocities in Problem (C), order/temperature [K] vs spatial [Å]*

In Figure 18, we plot order parameter and temperature along the z-axis for three different friction velocities. As expected, it indicates that a liquid layer forms in the middle, and also that the temperature is significantly higher at the friction interface than in the exterior of the domain.

5.3. Simulation of BPTI in Problem (D)

We equilibrate BPTI to 300°K at 1bar (NPT) for 210ps using a regular IM with an outer step size of 4fs. Afterwards, we switch to the CIM with an outer step size of 8fs and run at 300°K (NVT) for roughly 10 million steps, achieving

a simulation time of 80ns. This is still a very short trajectory, however, and major transitions happen on larger time scales [61, 62]. And yet, we could still observe small changes using the root-mean-square deviation (RMSD) as a reaction coordinate.

5.3.1. RMSD indicates two configurations

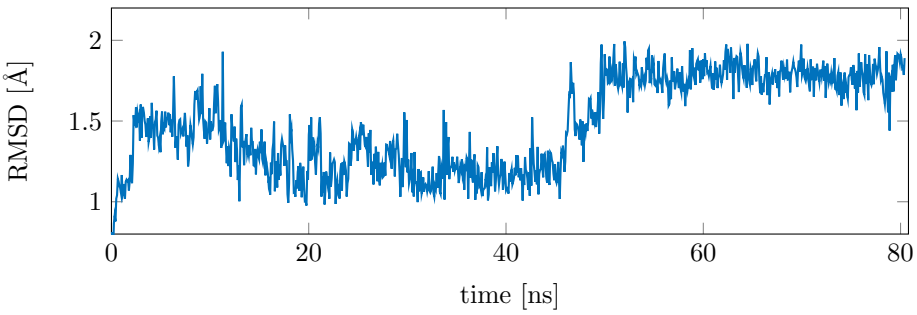

Figure 19: *BPTI in Problem (D): RMSD evolution over time [ns] for residues 5 to 54, backbone atoms only*

The RMSD is plotted in Figure 19 for backbone atoms of residues 5 to 54 versus time. After an initial equilibration, it seems to settle down just above 1Å until around 45ns. It then quickly moves to just below 2Å to find equilibrium again. In Figure 20, we plot the initial structure and snapshots after 39ns and 80ns. They indicate the origin of this behaviour: the lower left part of the backbone partially rotates. This is also supported by Figure 21, which shows the RMSD for each residue during those time frames. After 39ns, the structure is still relatively unchanged, as compared to the original. It is no surprise that the end tail clearly moves. There is an additional small peak at id 38 which indicates changes near the middle of the protein chain. Towards 80ns, the start tail also unfolds. More interestingly, residues 10 to 15 flip and move away from the center.

6. Conclusions

For biomolecular simulations with flexible bonds and angles, our new filter based on corotation successfully avoids resonance instabilities which inherently limit the impulse method. With our method, it is possible to use step sizes which are twice as large as those which can be used in the standard impulse method. It is stable, reliable and computationally cheap. The filter is most effective in simulations with expensive long-range calculations where we can obtain approximately 20% speed-up at no visible loss of accuracy. Its major advantage, compared to other filters, is its ease in implementation and its versatility.

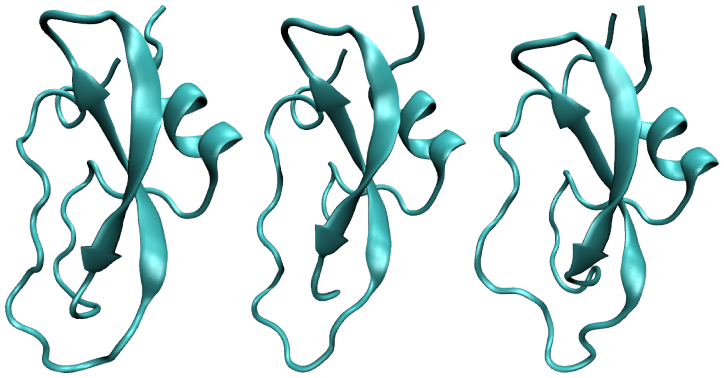

Figure 20: *BPTI snapshots from Problem (D) after approx. 0ns, 39ns and 80ns simulation time*

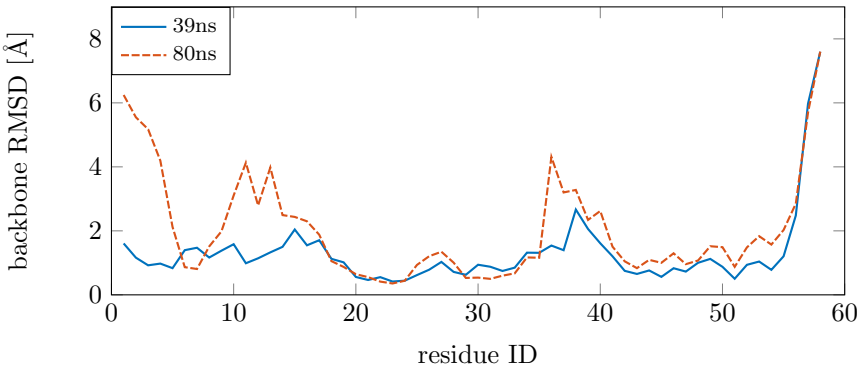

Figure 21: *Backbone RMSD per residue averaged over 800ps at 39ns and 80ns simulation time for BPTI in Problem (D)*

7. Acknowledgments

We thank the reviewer for the thorough review and highly appreciate the comments and suggestions, which significantly contributed to improving the quality of this paper. The authors are grateful to Volker Grimm for valuable comments and suggestions, and to Brianna Robinson for proofreading. This research was partially supported by a scholarship from the DAAD (German Academic Exchange Service). Most simulations were performed on the computational resource bwUniCluster funded by the Ministry of Science, Research and the Arts Baden-Württemberg and the Universities of the State of Baden-Württemberg, Germany, within the framework program bwHPC. Some computations were also performed on the gpc supercomputer at the SciNet HPC Consortium. SciNet[63] is funded by: the Canada Foundation for Innovation under the auspices of Compute Canada; the Government of Ontario; Ontario Research Fund - Research Excellence; and the University of Toronto.

References

[1] T. Schlick, Molecular Modeling and Simulation: An Interdisciplinary Guide, 2010.

[2] B. Leimkuhler, S. Reich, Simulating Hamiltonian Dynamics, Vol. 14, Cambridge University Press, 2004.

[3] M. Griebel, S. Knapek, G. Zumbusch, Numerical Simulation in Molecular Dynamics: Numerics, Algorithms, Parallelization, Applications, 1st Edition, Springer Publishing Company, Incorporated, 2007.

[4] B. J. Berne, Molecular Dynamics in Systems with Multiple Time Scales: Reference System Propagator Algorithms, Springer Berlin Heidelberg, Berlin, Heidelberg, 1999, pp. 297–317. doi:10.1007/978-3-642-58360-5_16.

[5] D. D. Humphreys, R. a. Friesner, B. J. Berne, A Multiple-Time-Step Molecular Dynamics Algorithm for Macromolecules, J. Phys. Chem. 98 (27) (1994) 6885–6892. doi:10.1021/j100078a035.

[6] R. Zhou, B. J. Berne, A New Molecular Dynamics Method Combining the Reference System Propagator Algorithm with a Fast Multipole Method for Simulating Proteins and Other Complex Systems, J. Chem. Phys. 103 (21) (1995) 9444–9459. doi:10.1063/1.470006.

[7] T. Schlick, Some Failures and Successes of Long-Timestep Approaches to Biomolecular Simulations, Springer Berlin Heidelberg, Berlin, Heidelberg, 1999, pp. 227–262. doi:10.1007/978-3-642-58360-5_13.

[8] R. D. Skeel, Integration Schemes for Molecular Dynamics and Related Applications, in: Grad. Student's Guid. to Numer. Anal. '98, 1999, pp. 119–176. doi:10.1007/978-3-662-03972-4_4.

[9] H. Grubmüller, H. Heller, A. Windemuth, K. Schulten, Generalized Verlet Algorithm for Efficient Molecular Dynamics Simulations with Long-range Interactions, Mol. Simul. 6 (1-3) (1991) 121–142. doi:10.1080/08927029108022142.

[10] M. Tuckermar, G. J. Martyna, B. J. Berne, Reversible multiple time scale molecular dynamics, J. Chem. Phys. 97 (3) (1992) 1990–2001. doi:10.1063/1.463137.

[11] T. C. Bishop, R. D. Skeel, K. Schulten, Difficulties with Multiple Time Stepping and Fast Multipole Algorithm in Molecular Dynamics, J. Comput. Chem. 18 (14) (1997) 1785–1791. doi:10.1002/(SICI)1096-987X(19971115)18:14<1785::AID-JCC7>3.0.CO;2-G.

[12] J. J. Biesiadecki, R. D. Skeel, Dangers of multiple time step methods, J. Comput. Phys. 109 (2) (1993) 318–328. doi:10.1006/jcph.1993.1220.

[13] T. Schlick, M. Mandziuk, R. D. Skeel, K. Srinivas, Nonlinear resonance artifacts in molecular dynamics simulations, J. Comput. Phys. 140 (1) (1998) 1–29. doi:10.1006/jcph.1998.5879.

[14] Q. Ma, J. Izaguirre, R. Skeel, Verlet-I/r-RESPA/Impulse is limited by nonlinear instabilities, SIAM J. Sci. Comput. 24 (6) (2003) 1951–1973. doi:10.1137/S1064827501399833.

[15] R. D. Skeel, J. A. Izaguirre, The Five Femtosecond Time Step Barrier, Springer Berlin Heidelberg, Berlin, Heidelberg, 1999, pp. 318–331. doi:10.1007/978-3-642-58360-5_17.

[16] J. a. Morrone, R. Zhou, B. J. Berne, Molecular Dynamics with Multiple Time Scales: How to Avoid Pitfalls, J. Chem. Theory Comput. 6 (6) (2010) 1798–1804. doi:10.1021/ct100054k.

[17] P. Minary, M. E. Tuckerman, G. J. Martyna, Long Time Molecular Dynamics for Enhanced Conformational Sampling in Biomolecular Systems, Phys. Rev. Lett. 93 (15) (2004) 150201. doi:10.1103/PhysRevLett.93.150201.

[18] I. P. Omelyan, A. Kovalenko, Overcoming the Barrier on Time Step Size in Multiscale Molecular Dynamics Simulation of Molecular Liquids, J. Chem. Theory Comput. 8 (1) (2012) 6–16. doi:10.1021/ct200157x.

[19] B. Leimkuhler, D. T. Margul, M. E. Tuckerman, Stochastic, resonance-free multiple time-step algorithm for molecular dynamics with very large time steps, Mol. Phys. 111 (22-23) (2013) 3579–3594. arXiv:1307.1167, doi:10.1080/00268976.2013.844369.

[20] M. E. Tuckerman, C. J. Mundy, G. J. Martyna, On the classical statistical mechanics of non-Hamiltonian systems, Europhys. Lett. 45 (2) (2007) 149–155. doi:10.1209/epl/i1999-00139-0.

[21] M. E. Tuckerman, Y. Liu, G. Ciccotti, G. J. Martyna, Non-Hamiltonian molecular dynamics: Generalizing Hamiltonian phase space principles to non-Hamiltonian systems, J. Chem. Phys. 115 (4) (2001) 1678–1702. doi:10.1063/1.1378321.

[22] J.-P. Ryckaert, G. Ciccotti, H. J. Berendsen, Numerical integration of the cartesian equations of motion of a system with constraints: molecular dynamics of n-alkanes, J. Comput. Phys. 23 (3) (1977) 327–341. doi:10.1016/0021-9991(77)90098-5.

[23] H. C. Andersen, Rattle: A "velocity" version of the shake algorithm for molecular dynamics calculations, J. Comput. Phys. 52 (1) (1983) 24–34. doi:10.1016/0021-9991(83)90014-1.

[24] E. Barth, T. Schlick, Overcoming stability limitations in biomolecular dynamics. I. Combining force splitting via extrapolation with Langevin dynamics in LN, J. Chem. Phys. 109 (5) (1998) 1617–1632. doi:10.1063/1.476736.

[25] G. H. Zhang, T. Schlick, Lin - a New Algorithm To Simulate the Dynamics of Biomolecules By Combining Implicit-Integration and Normal-Mode Techniques, J. Comput. Chem. 14 (10) (1993) 1212–1233. doi:10.1002/jcc.540141011.

[26] J. a. Morrone, T. E. Markland, M. Ceriotti, B. J. Berne, Efficient multiple time scale molecular dynamics: Using colored noise thermostats to stabilize resonances, J. Chem. Phys. 134 (1) (2011) 014103. arXiv:arXiv:1008.5377v1, doi:10.1063/1.3518369.

[27] B. García-Archilla, J. M. Sanz-Serna, R. D. Skeel, Long-Time-Step Methods for Oscillatory Differential Equations, SIAM J. Sci. Comput. 20 (3) (1998) 930–963. doi:10.1137/S1064827596313851.

[28] J. A. Izaguirre, D. P. Catarello, J. M. Wozniak, R. D. Skeel, Langevin stabilization of molecular dynamics, J. Chem. Phys. 114 (5) (2001) 2090. doi:10.1063/1.1332996.

[29] Q. Ma, J. A. Izaguirre, Targeted Mollified Impulse: A Multiscale Stochastic Integrator for Long Molecular Dynamics Simulations, Multiscale Model. Simul. 2 (1) (2003) 1–21. doi:10.1137/S1540345903423567.

[30] J. A. Izaguirre, S. Reich, R. D. Skeel, Longer time steps for molecular dynamics, The Journal of Chemical Physics 110 (20) (1999) 9853–9864. doi:http://dx.doi.org/10.1063/1.478995.

[31] S. Reich, Multiple Time Scales in Classical and Quantum–Classical Molecular Dynamics, J. Comput. Phys. 151 (1) (1999) 49–73. doi:10.1006/jcph.1998.6142.

[32] J. M. Sanz-Serna, Mollified Impulse Methods for Highly Oscillatory Differential Equations, SIAM J. Numer. Anal. 46 (2) (2008) 1040–1059. doi:10.1137/070681636.

[33] J. A. Izaguirre, Q. Ma, T. Matthey, J. Willcock, T. Slabach, B. Moore, G. Viamontes, Overcoming Instabilities in Verlet-I/r-RESPA with the Mollified Impulse Method, Springer Berlin Heidelberg, Berlin, Heidelberg, 2002, pp. 146–174. doi:10.1007/978-3-642-56080-4_7.

[34] T. Schlick, R. D. Skeel, A. T. Brunger, L. V. Kalé, J. a. Board, J. Hermans, K. Schulten, Algorithmic Challenges in Computational Molecular Biophysics, J. Comput. Phys. 151 (1) (1999) 9–48. doi:10.1006/jcph.1998.6182.

[35] D. A. Case, T. E. Cheatham, T. Darden, H. Gohlke, R. Luo, K. M. Merz, A. Onufriev, C. Simmerling, B. Wang, R. J. Woods, The Amber biomolecular simulation programs, J. Comput. Chem. 26 (16) (2005) 1668–1688. doi:10.1002/jcc.20290.

[36] B. R. Brooks, R. E. Bruccoleri, B. D. Olafson, D. J. States, S. Swaminathan, M. Karplus, CHARMM: A program for macromolecular energy, minimization, and dynamics calculations, J. Comput. Chem. 4 (2) (1983) 187–217. doi:10.1002/jcc.540040211.

[37] C. Oostenbrink, A. Villa, A. E. Mark, W. F. Van Gunsteren, A biomolecular force field based on the free enthalpy of hydration and solvation: The GROMOS force-field parameter sets 53A5 and 53A6, J. Comput. Chem. 25 (13) (2004) 1656–1676. doi:10.1002/jcc.20090.

[38] G. A. Kaminski, R. A. Friesner, J. Tirado-Rives, W. L. Jorgensen, Evaluation and reparametrization of the OPLS-AA force field for proteins via comparison with accurate quantum chemical calculations on peptides, J. Phys. Chem. B 105 (28) (2001) 6474–6487. doi:10.1021/jp003919d.

[39] S. Plimpton, Fast Parallel Algorithms for Short – Range Molecular Dynamics, J. Comput. Phys. 117 (June 1994) (1995) 1–19. doi:10.1006/jcph.1995.1039.

[40] S. Riniker, J. R. Allison, W. F. van Gunsteren, On developing coarse-grained models for biomolecular simulation: a review, Phys. Chem. Chem. Phys. 14 (36) (2012) 12423. doi:10.1039/c2cp40934h.

[41] E. Brini, E. a. Algaer, P. Ganguly, C. Li, F. Rodríguez-Ropero, N. F. a. V. D. Vegt, Systematic coarse-graining methods for soft matter simulations – a review, Soft Matter 9 (7) (2013) 2108–2119. doi:10.1039/C2SM27201F.

[42] A. Jain, N. Vaidehi, G. Rodriguez, A fast recursive algorithm for molecular dynamics simulation, J. Comput. Phys. 106 (2) (1993) 258–268. doi:10.1016/S0021-9991(83)71106-X.

[43] N. Vaidehi, A. Jain, Internal coordinate molecular dynamics: A foundation for multiscale dynamics, J. Phys. Chem. B 119 (4) (2015) 1233–1242. doi:10.1021/jp509136y.

[44] M. Müller, J. Dorsey, L. McMillan, Stable Real-time Deformations, Proc. 2002 ACM SIGGRAPH/Eurographics Symp. Comput. Animat. (2002) 49 – 54doi:10.1145/545261.545269.

[45] K. Röttger, A. Endriss, J. Ihringer, S. Doyle, W. F. Kuhs, Lattice constants and thermal expansion of H2Oand D2O Ice Ih between 10 and 265 K, Acta Crystallogr. Sect. B Struct. Sci. 50 (6) (1994) 644–648. doi:10.1107/S0108768194004933.

[46] M. Chaplin, Water Structure and Science, [Online; accessed 2015-11-13] (2015).
URL http://www1.lsbu.ac.uk/water/models.html

[47] O. Teleman, B. Jönsson, S. Engström, A molecular dynamics simulation of a water model with intramolecular degrees of freedom, Mol. Phys. 60 (1) (1987) 193–203. doi:10.1080/00268978700100141.

[48] M. a. González, J. L. F. Abascal, A flexible model for water based on TIP4P/2005, J. Chem. Phys. 135 (22) (2011) 0–8. doi:10.1063/1.3663219.

[49] A. MacKerell, D. Bashford, All-atom empirical potential for molecular modeling and dynamics studies of proteins, J. Phys. Chem. B 5647 (97) (1998) 3586–3616. doi:10.1021/jp973084f.

[50] M. M. Conde, C. Vega, a. Patrykiejew, The thickness of a liquid layer on the free surface of ice as obtained from computer simulation., J. Chem. Phys. 129 (1) (2008) 014702. arXiv:0901.1844, doi:10.1063/1.2940195.

[51] P. B. Louden, J. D. Gezelter, Simulations of solid-liquid friction at ice-I(h)/water interfaces., J. Chem. Phys. 139 (19) (2013) 194710. doi:10.1063/1.4832378.

[52] N. Samadashvili, B. Reischl, T. Hynninen, T. Ala-Nissilä, a. S. Foster, Atomistic simulations of friction at an ice-ice interface, Friction 1 (3) (2013) 242–251. doi:10.1007/s40544-013-0021-3.

[53] E. M. Schulson, A. L. Fortt, Friction of ice on ice, J. Geophys. Res. 117 (B12) (2012) B12204. doi:10.1029/2012JB009219.

[54] N. Maeno, M. Arakawa, A. Yasutome, N. Mizukami, S. Kanazawa, Ice-ice friction measurements, and water lubrication and adhesion-shear mechanisms, Can. J. Phys. 81 (2003) 241. doi:10.1139/P03-023.

[55] M. Marquart, J. Walter, J. Deisenhofer, W. Bode, R. Huber, The geometry of the reactive site and of the peptide groups in trypsin, trypsinogen and its complexes with inhibitors, Acta Crystallographica Section B 39 (4) (1983) 480–490. doi:10.1107/S010876818300275X.

[56] W. Humphrey, A. Dalke, K. Schulten, VMD: Visual molecular dynamics, J. Mol. Graph. 14 (1) (1996) 33–38. doi:10.1016/0263-7855(96)00018-5.

[57] A. Stukowski, Visualization and analysis of atomistic simulation data with OVITO–the Open Visualization Tool, Model. Simul. Mater. Sci. Eng. 18 (1) (2010) 015012.
URL http://stacks.iop.org/0965-0393/18/i=1/a=015012

[58] E. Hairer, C. Lubich, G. Wanner, Geometric numerical integration: structure-preserving algorithms for ordinary differential equations, Vol. 31, 2006.

[59] W. M. Brown, P. Wang, S. J. Plimpton, A. N. Tharrington, Implementing molecular dynamics on hybrid high performance computers – short range forces, Comput. Phys. Commun. 182 (4) (2011) 898–911. doi:10.1016/j.cpc.2010.12.021.

[60] J. R. Errington, P. G. Debenedetti, Relationship between structural order and the anomalies of liquid water., Nature 409 (6818) (2001) 318–21. doi:10.1038/35053024.

[61] D. E. D. Shaw, P. Maragakis, K. Lindorff-Larsen, S. Piana, R. O. Dror, M. P. Eastwood, J. a. Bank, J. M. Jumper, J. K. Salmon, Y. Shan, W. Wriggers, Atomic-Level Characterization of the Structural Dynamics of Proteins, Science 330 (October) (2010) 341–346. doi:10.1126/science.1187409.

[62] M. Gur, E. Zomot, I. Bahar, Global motions exhibited by proteins in micro- to milliseconds simulations concur with anisotropic network model predictions, J. Chem. Phys. 139 (12) (2013) 121912. doi:10.1063/1.4816375.

[63] C. Loken, D. Gruner, L. Groer, R. Peltier, N. Bunn, M. Craig, T. Henriques, J. Dempsey, C.-H. Yu, J. Chen, L. J. Dursi, J. Chong, S. Northrup, J. Pinto, N. Knecht, R. V. Zon, SciNet: Lessons Learned from Building a Power-efficient Top-20 System and Data Centre, J. Phys. Conf. Ser. 256 (2010) 012026. doi:10.1088/1742-6596/256/1/012026.